Appearance Potentials of Field Desorbed Silver Ions

E. Hummel, M. Domke**, and J. H. Block*
Fritz-Haber-Institut der Max-Planck-Gesellschaft

Z. Naturforsch. **34a**, 46–54 (1978); received November 3, 1978

Dedicated to Prof. Dr. Dr. h.c. mult. Georg-Maria Schwab on the occasion of his 80. birthday

The onset, $e\delta_0$, in the energy distribution of field desorbed silver ions (from Ag deposit on a W-tip) has been measured at $T > 400$ K. With increasing field strength ($0.5 \cdot 10^{10}$ V/m $< F <$ $1 \cdot 10^{10}$ V/m) or with decreasing temperature (800 K $> T >$ 500 K), $e\delta_0$ increases up to 1.5 eV. For a comparison with the $e\delta_0$-values, activation energies, Q, for field desorption have been determined from Arrhenius plots (0.5 eV $< Q <$ 2 eV). Two different kinetic regimes (desorption and diffusion) were identified. For field desorption, the sum $e\delta_0 + Q$ is constant, irrespective of F-values.

In the frame of "image hump" or "charge exchange" models, field dependent activation barriers are discussed. Temperature dependencies are related to (i) the Fermi distribution of the emitter, (ii) the distribution of F and (iii) the distribution of surface bond energies. Results are consistently explained in a three-dimensional model with directionally distinguished desorption steps.

1. Introduction

Field desorption (FD) and field evaporation (FEV) processes are governed by the bond strength of surface atoms. The electric field in front of the surface reduces the potential barrier for ion desorption. The binding energy can thus be compensated by electrostatic forces or, at elevated temperatures, partially by thermal activation. Two models have been developed to describe these processes: The "image hump" model [1], regarding the transition of a pre-formed ion over the Schottky barrier in front of the surface, and the "charge exchange" model [2], considering the intersection point of the neutral's and ion's potential curve. In earlier work [3] the desorption field strength has been used to evaluate surface bond strengths within the frame of the image hump model. Recently, field ion appearance potential spectroscopy (FIAPS) has been proven to be a much more direct method to evaluate bond energies [4, 5]. Furthermore, these measurements permit to explore the dynamics of desorption processes in greater detail. In the present investigation, we raise the question how, at elevated temperatures, competition between electrostatic forces and thermal activation in the desorption process can be studied by FIAPS.

2. Appearance Potentials

In analogy to field ionization (FI) in the gas phase [6], FD and FEV can be investigated by measuring the energy distribution of the desorption products. A charged ion is desorbed with a minimum "critical energy deficit", ΔE_c, being determined (in the example of Fig. 1) by the potential difference between the surface vacuum level and the point at distance x_c, where atomic and ionic potential curves are crossing

$$\Delta E_c = I - \Phi_E + (\Lambda + E_{pa}) - Q(F)\,. \qquad (1)$$

I is the ionization energy, Φ_E the emitter work function, Λ the field free binding energy, E_{pa} the atom's polarization energy and Q the field (F)-dependent activation energy of FD or FEV.

The integral distribution of kinetic energies is obtained by the application of retarding potentials. The high energy onset of the distribution is affected by the maximum measurable kinetic energy of the particles at the moment of field desorption. Thermally desorbed neutrals usually are expected with a Maxwellian distribution for the surface temperature T_s; deviations from the statistical mean value of the Maxwell distribution, $2kT_s$, up to a factor of 2 are possible [7, 8]. Assuming similar influences on FD, the kinetic energy of field desorbed ions should cause measurable tails zkT_s in the field ion energy distribution (the factor z, describing to which extent the distribution will be measured, depends on the signal to noise ratio S/N, and has values of $z \approx 10$ at a typical $S/N \approx 10^3$). The temperature dependent tail of this distribution is further enlarged by tunneling processes into vacant electronic states which at higher temperature T_s are successively depleted

* To whom enquiries should be sent.
** Present address: Institut für Atom- und Festkörper-Physik, Freie Universität Berlin.

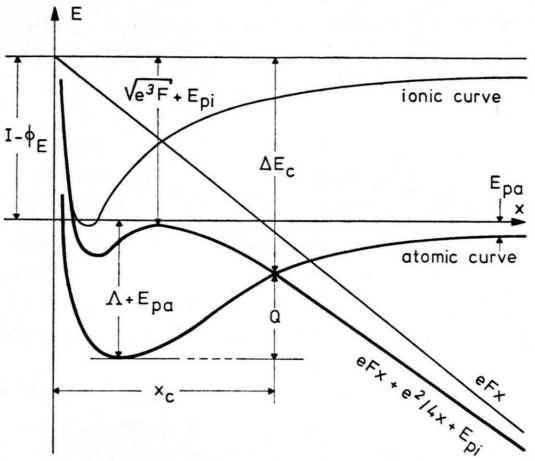

Fig. 1. Potential of a neutral and an ionic particle in front of a surface, describing the field desorption process. At infinite distance from the surface ($x\to\infty$), atomic and ionic potential curves differ in energy by $I-\Phi_E$. At equilibrium distance, the surface interaction consists of the atomic binding energy Λ and an additional field induced term E_{pa}. The transition from atomic to ionic state may occur at the crossing point ("charge exchange") at distance x_c. The field desorption process is then determined by the activation energy Q and the critical energy deficit ΔE_c.

below the Fermi level [6]. This results in an additional temperature term in $z k T_s$.

Experimentally, the onset $e\delta_0$ of the energy distribution is obtained by balancing emitter and retarder potential by the potential difference δ_0 at vanishing counting rate. The retarder consists of a grid having the work function Φ_R. The potential difference δ_0 is maintained by a battery between the Fermi levels of retarder and emitter. Therefore the experimental value of $e\delta_0$ contains the difference in contact potentials of emitter and retarder, $\Phi_E-\Phi_R$. Thus, $\Delta E_c+\Phi_E$ in (1) is substituted by $e\delta_0+\Phi_R$. Taking further contributions from surface temperature into account, we obtain:

$$e\delta_0 = I-\Phi_R+(\Lambda+E_{pa})-Q(F)-z k T_s. \quad (2)$$

The retarder work function, Φ_R, as a calibration constant, is usually obtained from low temperature rare gas FIAPS [6]. The appearance potential, AP, which should be independent of the apparatus, is accordingly defined as

$$\begin{aligned} AP &= e\delta_0+\Phi_R = \Delta E_c+\Phi_E-z k T_s \\ &= I+(\Lambda+E_{pa})-Q(F)-z k T_s. \end{aligned} \quad (3)$$

For ionic adsorbates, (2) reads [9]

$$\begin{aligned} e\delta_0 = \Phi_E-\Phi_R+(\Lambda_i+E_{pi}+eFx_0) \\ -Q_i(F)-z k T_s, \end{aligned} \quad (4)$$

where Λ_i, the binding energy of the ion, is referred to a field free ion energy at infinity. $Q_i(F)$ is the activation energy of the ion desorption. The potential energy curve of the ion is further affected by the ion's polarization energy E_{pi}, and the field energy term eFx_0 at the equilibrium distance x_0.

The resulting field dependent potential barrier Q prevents immediate desorption. Neglecting tunneling, which is important only at low temperatures [10], this potential barrier can be evaluated by independent rate measurements, in accordance with the Arrhenius equation

$$k = k_0\exp(-Q/kT). \quad (5)$$

The position of the barrier differs in the "image hump" and "charge exchange" model, as described in the literature. In the image hump model the atomic state is first transferred into the ionic state, and the ion still has to overcome the Schottky saddle. The activated process of field desorption is the transition of an ion across the Schottky hump, which can be determined by the ion's potential curve. For particles being adsorbed in ionic form on a metal surface, the same Schottky barrier applies without any preceding charge transition. In the charge exchange model, as demonstrated in Fig. 1, the ion is formed and desorbed at the intersection of the atomic and ionic potential curves. If the intersection is closer to the surface than the Schottky saddle, the process can be approached by the image hump formalism. Here, the ionic curve is represented by the image force, neglecting repulsive forces or any surface interaction. Thus ΔE_c can be evaluated explicitly as

$$\Delta E_c = \sqrt{(4\pi\varepsilon_0)^{-1}e^3F}+E_{pi}. \quad (6)$$

Disregarding the correction term E_{pi}, we find the critical energy deficit directly proportional to the square root of the field strength. The onset of the measured energy distribution accordingly is

$$\begin{aligned} e\delta_0 = \Phi_E-\Phi_R+\sqrt{(4\pi\varepsilon_0)^{-1}e^3F} \\ +E_{pi}-z k T_s. \end{aligned} \quad (7)$$

The charge exchange model usually displays a stronger F-dependence of ΔE_c depending on the shape of the interaction potential.

3. The Ag/W System

Especially at higher temperatures, it is usually difficult to maintain a stable field desorption current for extended times, since diffusion and

desorption processes affect the local radius of curvature and field strength. In order to avoid these difficulties, a tungsten emitter was chosen as a stable support, whereon silver was deposited and heated for sufficient surface mobility prior to desorption, FD or FEV.

At low coverages, the Ag-W interaction will determine the bond strength. With increasing coverage, Ag–Ag bonds are involved. The sublimation energy of silver amounts to 2.9 eV [11]; for the adsorption energy of Ag on W different values have been reported in the literature. Rate measurements, mainly controlled by field electron emission, reveal two adsorption states at lower and at higher coverage. Measured values for respective states are given as 1.8 and 1.6 eV [12] or 2.8 and 2.0 eV [13] or, on (110) W, 2.86 and 1.78 eV [14]. The adsorption energy was found to depend sensitively on contamination, decreasing from 2.9 eV to 2.06 after oxygen deposit [15]. Thermal desorption measurements [16] yield energies that change with increasing coverage of Ag (3.06 to 4.7 eV to 4.0 eV on (110) W; 4.55 to 2.1 to 2.9 eV on (100) W). All these energies differ remarkably and are at variance according to whether Ag–Ag or Ag–W is the stronger bond.

The influence of silver adsorption on the work function of tungsten shows that neutral particles predominate, since alterations in Φ reported are ± 0.4 eV [12, 13, 17]. Accordingly, the Saha-Langmuir equation predominantly requires neutrals in thermal desorption (with $I = 7.57$ eV and $\Phi_E = 4.5$ eV). For the activation energy of diffusion, E_{diff}, values of 0.8 eV [13] and of 0.55 eV at coverage $\Theta < 1$ and 0.43 at $\Theta > 1$ [12] are reported; at 300 to 400 K appreciable diffusion is observed.

4. Experimental

The apparatus, as described in detail elsewhere [6], consists of a field ion source (tungsten tip and a counter-electrode), a focusing lens system, a gold mesh retarder, a quadrupole mass analyzer and a single particle counting device. Integral energy distributions are obtained by varying the potential difference δ between emitter and retarder. The distribution onset $e\delta_0$ for rare gases at low temperature is determined with an accuracy of ± 0.02 eV. The calibration constant, Φ_R, is determined from time to time from 80 K rare gas FI measurements in order to ascertain effects mainly due to adsorption on the retarder grid. In fact, Φ_R after bake out increased during a period of several months from 4.1 to 4.4 eV.

The tip was thoroughly cleaned by degassing at $T > 2500$ K and by field desorption; its cleanness could be controlled by field electron micrographs observed at the phosphorous screen on the counter-electrode. The tip temperature is determined from the resistance of the supporting heating loop. Field strength data are taken from Fowler-Nordheim plots.

Vaporous silver, originating from a Knudsen cell, was deposited on the tip, situated nearly perpendicular to the atom beam axis at a distance of 5 cm. The Knudsen cell is a d.c. heated Ta tube having a 0.5 mm hole. Its temperatures are estimated pyrometrically; values up to 1600 K can be achieved with heating currents > 100 A. Equilibrium pressures of 7 Pa (0.05 Torr) are established in the cell at temperature values typically 1400 K; the flux of the silver beam at the tip position is $4 \cdot 10^{14}$ cm^{-2} s^{-1}, equivalent to a "pressure" of $7 \cdot 10^{-4}$ Pa ($5 \cdot 10^{-6}$ Torr).

Appearance potentials of field desorbed silver ions were also measured at various tip temperatures with particle supply from the shank, while the Knudsen cell was switched off.

5. Field Ionization of Silver Vapor

Free silver atoms can be field ionized in two different ways, (i) by directing a silver beam from the Knudsen cell (temperature T_g) into the high field area in front of the tip, or (ii) by thermal desorption of silver atoms from the emitter (at $T_s > 800$ K) and subsequent ionization of silver vapor atoms. The first method displays results with rather high noise, due to the glowing Knudsen cell. In the second method, data on field ionization of silver atoms are superimposed by data of field evaporation processes. Field ionization of gaseous atoms yields energy distribution onsets [6]

$$e\,\delta_0 = I - \Phi_R - z\,kT_g\,, \tag{8}$$

while field evaporation processes are expected to be described by (2). As demonstrated earlier for gas phase ionization [6], ionization energy I and AP values should differ only in the temperature term zkT. The experimental results of the silver vapor measurements are compiled in Table 1; Φ_R values

Table 1. Field ionization AP data in [eV] of vaporous Ag obtained by Knudsen cell vaporization (1) and by thermal desorption from tip (2); for comparison: $I_{Ag} = 7.57$ eV.

	$T = 750$ to 800 K	$T \approx 1300$ K	$T \approx 1500$ K
(1) AP_{vap}		7.12 – 7.2	7.07
(2) AP_{des}	7.45 – 7.75		

were taken from rare gas field ionization at 80 K. Field ionization of the atomic beam (method 1) yields AP_{vap}-values which are 0.4 to 0.5 eV smaller than ionization potentials. The difference $(I - AP_{vap})$ ranges within the expected temperature correction zkT_g, the temperature dependence between 1300 and 1500 K remaining within the error limits. The second method gives $(I - AP_{des})$ values near zero, which means that temperature corrections are nearly compensated by other energy losses.

6. Field Desorption at Different Field Strengths and Temperatures

At moderate field strength ($F < 1.5 \cdot 10^{10}$ V/m), only Ag^+ ions are field desorbed from a silver covered tungsten tip. Doubly or higher charged atoms or multiples could not be detected. According to Fig. 1, the integral energy distributions of desorbed silver ions should display strongly field dependent onsets, $e\delta_0$. There the temperature dependence should give zkT_s terms in accordance with (3). These correlations have been examined experimentally.

Usually, field desorption of silver from a precovered tungsten tip was measurable only at temperatures $T > 400$ K, which is just the temperature of beginning surface diffusion. This indicates that the ionization zone is supplied by surface diffusion of silver. Field effects on this surface diffusion, in form of reduced diffusion temperatures for instance have not been noticed, probably since the rate determining part of diffusion at remote regions of the shank proceeds in negligible field gradients. In this way, even totally depleted tips emit silver ions again after staying at room temperature for extended times (hours). Silver atoms must have diffused longer distances than observable in field emission microscopy on tungsten at 300 K and without the influence of an electric field.

The determination of field strength values involves certain problems. Usually, the field strength is obtained from Fowler-Nordheim plots at low temperatures. The adsorption of silver and the high temperature treatment of the emitter may alter the surface roughness and local field strength. In most of the present cases, adsorption and high temperature field desorption of silver changed the Fowler-Nordheim characteristics only to an extent which can be ascribed to work function variations up to 0.5 eV (Chapter 3). In these cases, the threshold voltage for rare gas field ionization at 80 K remained nearly unchanged after adsorption and heat treatment, indicating constant surface morphology.

Occasionally, the slope alteration in Fowler-Nordheim plots and increased electron current at lower voltages indicated growing surface roughness. At the same time, field desorption of silver ions was observed at lower temperatures, $T_s \approx 300$ K, and with higher energy deficits. This "state" of surface condition was not stable enough for measuring threshold voltages of rare gas field ionization. We ascribe this state to a "whisker"-like surface with increased field strength and field desorption without preceding surface diffusion. Results from these "whisker" states of the surface are compiled in Table 2. The field strength data F_W were derived from the shape of the supporting tungsten tip. Actual F-data of the silver surface are unknown, must however exceed those of the support. Because of the unknown work function variations and because of patch fields, Fowler-Nordheim plots also fail to determine field strength values.

The energy distributions for the normal ("whisker-free") state of the surface are shown in Figure 2. At constant field strength ($F = 0.6 \cdot 10^{10}$ V/m), the $e\delta_0$-values decrease with increasing temperature (Figure 2a). The slope of the onset curve decreases

Table 2. Appearance potentials of ions formed at "whisker" states of surfaces (energies in eV).

T	F_W[V/m]			
	0.54×10^{10}	0.68×10^{10}	0.88×10^{10}	1.02×10^{10}
300 K		9.6	9.5	9.4
350 K	9.4	9.4		
580 K	8.6			
780 K	7.6			

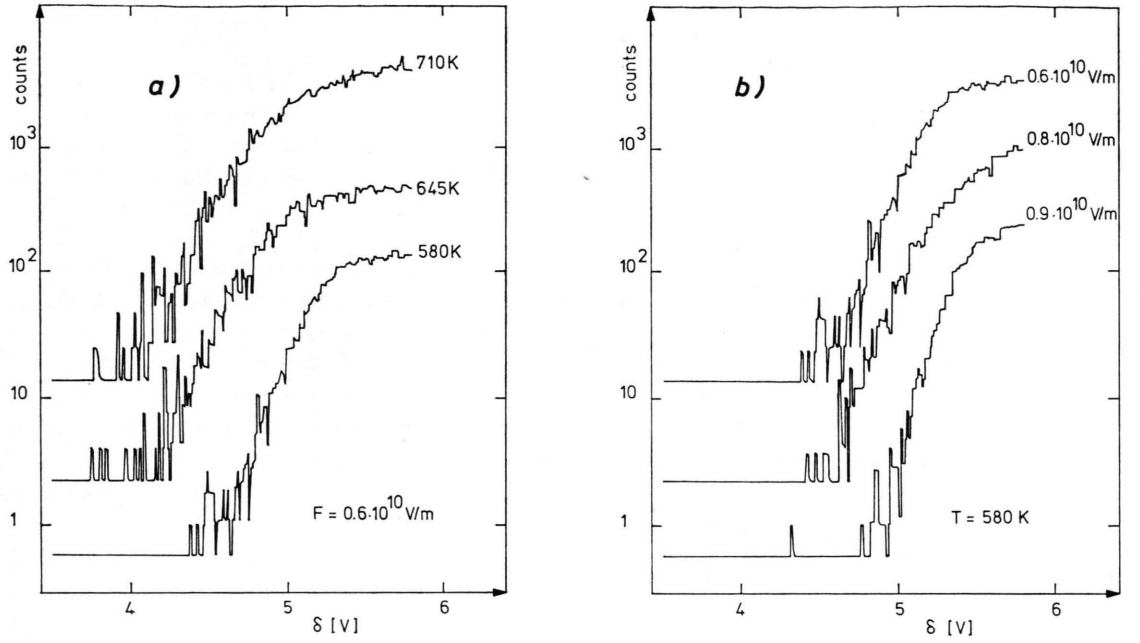

Fig. 2. Measured integral energy distributions of Ag^+ desorbed from tungsten, measured at different temperatures (a) and field strengths (b).

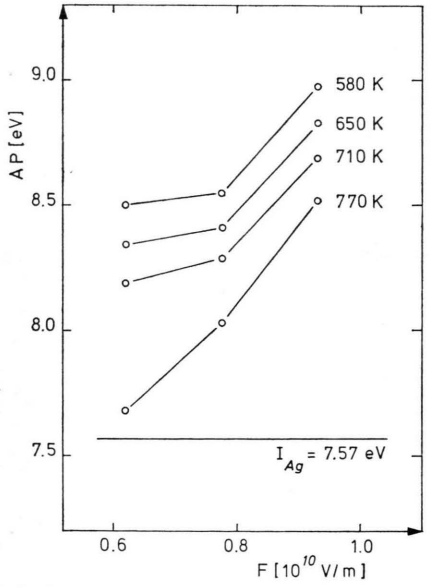

Fig. 3. AP-values of field desorbed silver as a function of field strength F at different surface temperatures T_S. Experimental inaccuracies of $e\delta_0$ increase with temperature and field strength; errors range between ± 0.02 and ± 0.05 eV. At the bottom, the ionization energy of silver, I_{Ag}, is shown. AP-values of thermally desorbed and subsequently ionized silver atoms are close to I_{Ag} (± 0.2 eV) and independent of field strength.

with increasing temperature. The field dependence of onset curves at constant temperature ($T = 580$ K) is shown in Fig. 2b. With increasing field strength, the onset curves shift to higher values of δ. The AP-values determined from different experiments at "whisker-free" surfaces are shown in Fig. 3. In all cases the AP-values increase with field strength, as expected from Fig. 1, and decrease with temperature, but much more than expected from (3). At high temperatures and low field strengths, the AP-values usually approached that of the gas phase ionization of Ag, I_{Ag}, as shown in Figure 3. These low AP-values could not be reproduced in all measurements. In one series of experiments, the AP-values at low field strength did not drop below 8.3 eV although the temperatures were raised to 850 K. Obviously, a certain state of deposit is required to reproduce the low AP-values of 7.6 to 8.5 eV observed at 770 K to 580 K, respectively.

For the understanding of details of the field desorption process, an independent measurement of the activation energy Q (Fig. 1) is of interest. This can be achieved by measuring the temperature dependencies of field evaporation rates and by determining activation energies from Arrhenius

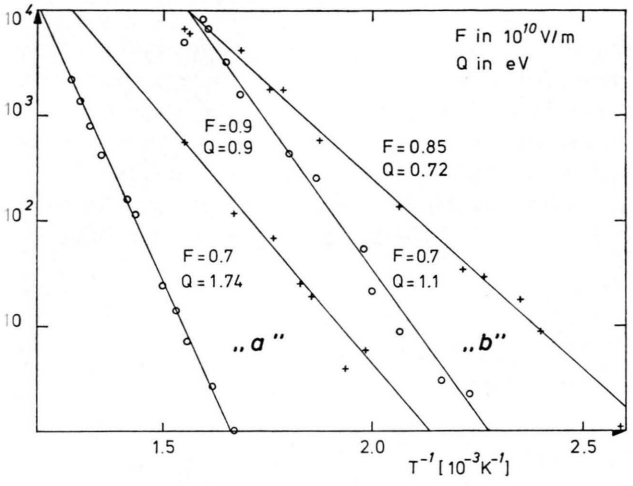

Fig. 4. Arrhenius plots of field desorbed silver ions. (Experimental data at $F = 0.9 \cdot 10^{10}$ V/m have to be multiplied by a factor 10). Evidently, the measurements denoted "a" reveal a steeper slope than those denoted "b".

plots. For those processes which can be quantitatively described by the potential energy diagram of Fig. 1, the sum of the AP-values and the measured activation energies should be constant, irrespective of actual field strength values.

The experimental data of rate measurements, as represented in Fig. 4, display a rather high degree of scattering. However, one can distinguish between two different "states", a and b, of the field evaporation process. Q-values are field dependent in any case, decreasing with increasing field. At similar fields, "state a" (left side in Fig. 4) always displayed twice the Q-value of "state b", where ion intensities always were higher.

The scatter of the experimental values in Fig. 4 may be due to local variations of ionization probabilities, bond energies, or supply problems which cannot be followed without FIM observations. From thermal desorption measurements, it is well known [18, 19] that activation energies as determined by rate measurements are frequently influenced by supply mechanisms. These influences may be even more pronounced in the present case, where the analysis of surface compounds is confined to small areas (of 1000 Å^2) at the apex of the emitter. We have to expect that rate determining steps of "state a" involve supply of Ag by surface diffusion. A desorption process, whose rate constant of desorption, k, is determined by the sum of the activation energies of desorption Q and diffusion E_{diff},

$$k = N \exp[-(E_{\text{diff}} + Q)/kT], \tag{9}$$

has recently been discussed for low coverages [20].

In the present case, the increase of activation energy at depletion of the adsorption layer may much more likely be caused by geometrical factors. At increased temperatures enlarged areas at remote distances will contribute to the supply of the tip apex.

For case "b", rate measurements at different temperatures could be related to subsequent AP measurements. The results shown in Fig. 5 indicate that the sum of AP and Q is almost constant. Since the AP-values decrease with temperature whereas the Q-values are invariant within experimental accuracy, each temperature displays a different constant. These different constants are still consistent with our model (Chapt. 8.2), since AP-values represent maximum energies of the distribution, while Q-values are mean values.

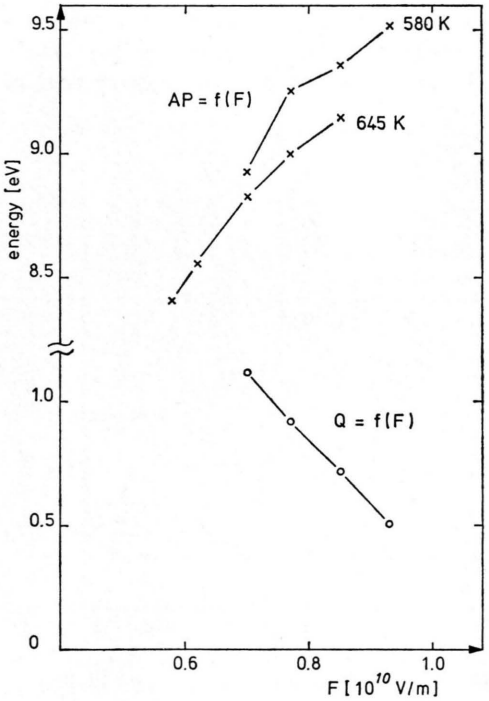

Fig. 5. Q-values from Arrhenius plots and AP-values, measured subsequently. According to (3), the sum of both is field independent ($AP + Q = 10.0$ eV at 645 K and 10.1 eV at 580 K).

7. Desorption of Potassium

In order to compare temperature effects, the thermal desorption of ionically adsorbed potassium was investigated under field-free conditions. For this purpose, a certain amount of potassium was adsorbed on the tungsten surface from an atomic beam source and subsequently thermally desorbed. During these measurements, only small focusing voltages (up to 30 V) were applied between tip and counter electrode. At negligible field strength, the bond energy Λ has to be supplied completely by thermal activation ($Q = \Lambda$). Literature data of the activation energy, as determined by Arrhenius plots, range between $Q = 2.0$ and $Q = 3.2$ eV [21, 22]. For potassium in ionic form (4) reduces to

$$e\,\delta_0 = \Phi_E - \Phi_R - z\,kT_s\,. \tag{10}$$

At constant Φ_E, the kinetic ("Maxwellian") part of zkT_s is equal to the shift of $e\,\delta_0$ with temperature. Experimental results (Fig. 6) clearly show increasing tails of the energy distributions at increasing temperatures. Since the desorption of preformed ions is measured, the temperature dependence of the Fermi distribution has no importance. At a typical signal to noise ratio of 10^2 during these measurements, a value of $z = 6.5$ is expected [6]. These calculated values are shown in the bottom part of Figure 6.

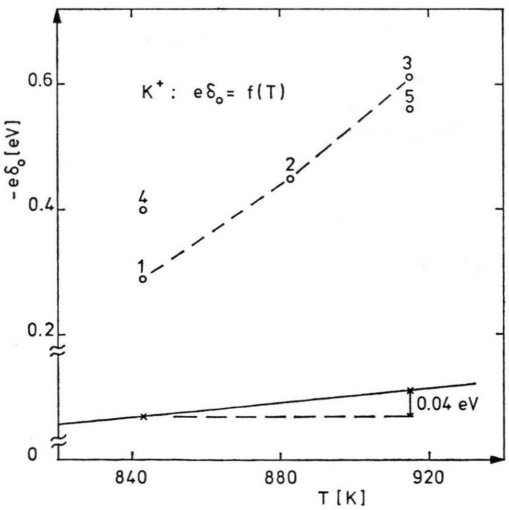

Fig. 6. The onset $e\delta_0$ of the measured energy distribution of K^+ versus tip temperature. For comparison, the expected temperature effect of the Maxwellian distribution is represented at the bottom ($S/N = 100$, $z = 6.5$). The sequence of measurements is indicated by numbers 1 to 5 and displays shifts due to changes in coverage and Φ_E.

The experiments yield $e\delta_0$-values with a drift, caused by time- and temperature-dependent K coverages and Φ_E-values (Figure 6). In spite of these uncertainties, the experimental slope seems to exceed the tail expected for a gas phase Maxwellian distribution. Thus, the experiments with potassium fail to set a standard for temperature effects at zero field and negligible surface interaction.

8. Discussion

8.1. The Field Dependence of AP

The measured field dependence of AP (Fig. 3) can directly be explained from the potential diagram (Figure 1). The results are in accordance with former measurements [5] of Ag at lower temperatures and higher field strengths and reflect the usual behavior of field desorption and field evaporation [23].

Considering the absolute values of the energy deficits within the frame of the image hump model (7), we can to a first approximation neglect the ion's polarization term, E_{pi}, and the temperature term zkT_s. At a field strength of $F = 1 \cdot 10^{10}$ V/m and a polarizability of $\alpha \approx 1$ Å^3 [24], the E_{pi} term is smaller than 0.04 eV. Influences of the temperature term will be discussed later. Under these suppositions the image hump, i.e. the maximum of the ionic curve, should differ from the measured $e\delta_0$-value only by the difference $\Phi_E - \Phi_R$, which can be estimated. The retarder work function drifted slightly with time, from $\Phi_R = 4.10 \pm 0.02$ eV in the early state of experiments to $\Phi_R = 4.40 \pm 0.02$ eV at the last measurements. Φ_E for a silver covered tungsten surface is taken from literature and from our own Fowler-Nordheim measurements. The values range from $\Phi_E = 4.0$ to 4.7 eV, according to silver coverage. Table 3 contains, for comparison, calculated Schottky barriers and measured $e\delta_0$-values. The deviation in these sets of data cannot be explained by contact potential differences. In addition, the temperature term ($T = 500$ K) zkT_s in (2) would add another 0.3 eV to the discrepancy. The same deviation between experiment and calculation, although smaller, had been observed in former results [5] at higher field strengths and lower temperatures.

The reason for this deviation may be the covalent bond part of the surface interaction. Thus, the image

Table 3. Comparison of ΔE_c-values calculated according to the "image hump" model, Eq.(6), with experimental data.

$F[10^{10}\,\mathrm{V/m}]$	$\sqrt{\frac{e^3F}{4\pi\varepsilon_0}}$ [eV] calc.	$e\delta_0$[eV] exp. this work $T_s = 580$ K	Ref[5] (Ag/Ag)
0.70	3.17	4.86	
0.77	3.33	5.19	
0.85	3.50	5.29	
0.93	3.66	5.45	
1.3	4.33		4.9
1.43	4.54		5.3
1.82	5.12		6.25

hump model must be modified by an additional covalent bonding part, added to the ion's potential curve. The other description, the charge exchange model, may be applied without modification. However, it is unlikely again that the ion's potential curve is only determined by field and image forces. This causes unknown variations in the ion's potential curve and again uncertainties in the exact position of the intersection point. For determining shapes of potentials at surfaces from energy deficit measurements, these effects have to be taken into account.

8.2. The Temperature Dependence of AP

The present understanding of temperature effects in AP, given in (3) by the term zkT_s, is restricted to the Maxwellian and Fermi energy distribution tails that have been measured and estimated in the case of gas phase ionization [6]. Here, AP typically (at a signal-to-noise ratio of 10^3) decreases by 0.1—0.2 eV at a temperature increase of approximately 200 K ($580 < T_s < 770$ K). On the other hand, the temperature effect measured for field desorbed silver amounts up to 0.9 eV (Figure 3). This amount cannot be explained by energy distributions, discussed so far for gas phase field ionization. Even in most favourable cases, i.e. electron tunneling from adsorbed particles with long residence times at distances smaller than x_c into unoccupied states below the Fermi level (at elevated T_s), temperature effects of this magnitude are not conceivable.

The one-dimensional models of the field desorption process are doubtlessly strongly simplified [25]. The non-isotropic spatial distribution of field desorbed particles [26, 27] indicates an obstruction of field desorption in certain directions and enhanced ion emission in others.

These observations may be considered in connection with earlier results concerning the pre-exponential factors of field evaporation rates [28, 29]. Experimental pre-exponentials were found several orders of magnitude smaller than expected for typical vibrational frequencies, indicating hindered desorption.

For Ge, a semiconductor having directed bonds, spatial effects in evaporation rates could directly by explained by a three-dimensional lattice model, displaying preferential evaporation directions [30].

Also in the present case, the field desorption of Ag^+, we will assume hindrance in certain evaporation directions at lower temperatures ($T_s < 600$ K). With a small pre-exponential factor, field evaporation will only be observed in directions where the barrier for desorption is sufficiently small. This barrier is given by the local potentials in front of the emitter. The directions of atomic or ionic trajectories along minimum energies are not necessarily determined by the direction of the external field. The superposition of the external field onto the local surface fields governs the desorption trajectories. Thermal activation will successively allow evaporation in other directions. At elevated temperatures, new desorption pathways are opened with higher barriers. At highest temperatures, where thermal desorption of neutrals is observed, evaporation (for subsequent gas phase ionization) will be an isotropic phenomenon.

At constant (external and local) fields, field desorption at elevated temperature may occur in directions, where the external field is not maximal, resulting in lower AP-values. The majority of desorption products, determining Q, still may be governed by maximum field directions.

The above model involves features which, in a one-dimensional model, can explain temperature effects only by two arguments, (i) a field strength distribution at the surface, and (ii) a distribution of surface bond energies.

(i) The field strength distribution, as for instance caused by deviations from spherical shape, would display different AP-values. With increasing external field, areas with larger radius of curvature can contribute and cause a larger distribution of AP-values. A field dependence of AP-values can only be measured if the field distribution excludes

permanent contributions from threshold fields. At increasing temperature, areas of lower field strength will successively contribute with accordingly diminished AP-values.

It is questionable whether such an initial field distribution is present in our experiments on Ag/W. Actually, there have been no changes observed after heat treatment and subsequent quenching of the emitter with respect to Fowler-Nordheim plots and threshold voltages of rare gas field ionization.

(ii) The bond energy, denoted Λ in Fig. 1, is not necessarily the sublimation energy as known from thermodynamics. Fig. 1 describes a bond energy that is actually present at the initial state of field desorption. There may be surface atoms of different coordination numbers, i.e. kink sites or adatoms. The bond energy at these sites is different, and since the measurements of AP reveal the last step, different Λ-values have to be considered in Figure 1. With increasing temperature, the population of less tightly bound surface atoms, for instance adatoms, is conceivable. As a consequence, a distribution of Λ-values is connected with a distribution of AP-values. At higher temperatures, lower AP-values are measured.

In the three dimensional model, a distribution of Λ-values has not necessarily to be assumed. The surface interaction, and consequently the potential barrier Q, changes with direction of desorption. Pathways with minimum Q-values are exclusively used for desorption at lower temperatures, higher activation barriers (high Q and low AP) can be surmounted at elevated temperatures. This again describes a temperature dependence of AP as a directional desorption effect, not necessarily involving initial distributions of Λ-values.

In the frame of this model, we can also understand the AP-values of silver coming from the shank of the emitter (Table 1). At elevated temperatures, silver atoms may migrate or evaporate and jump from the shank into the ionization zone. It is conceivable that gas-like but fully accommodated particles are ionized. Under these circumstances, Λ-values would have no importance, but the polarization term, E_{pa} (≈ 0.3 eV at $\alpha = 10$ Å^3 [31] and $F = 10^{10}$ V/m) would be involved, since atoms are accommodated to the emitter surface. For Ag^+, AP-values of ≈ 7.5 eV would be expected, as found experimentally (Figure 3).

Acknowledgements

Financial support of this work by the Deutsche Forschungsgemeinschaft, Bad Godesberg, is gratefully acknowledged.

[1] E. W. Müller, Phys. Rev. **102**, 618 (1956).
[2] R. Gomer, J. Chem. Phys. **31**, 341 (1959).
[3] E. W. Plummer and T. N. Rhodin, J. Chem. Phys. **49**, 3479 (1968).
[4] A. R. Waugh and M. J. Southon, J. Phys. D: Appl. Phys. **9**, 1017 (1976).
[5] T. T. Tsong, W. A. Schmidt, and O. Frank, Surf. Sci. **65**, 109 (1977).
[6] M. Domke, E. Hummel, and J. H. Block, Surf. Sci. **78**, 307 (1978).
[7] G. Comsa, Proc. 7th Int. Vac. Congr. a. 3rd Int. Conf. Solid Surf. Vienna 1977, p. 1317.
[8] A. E. Dabiri, T. J. Lee, and R. E. Stickney, Surf. Sci. **26**, 522 (1971).
[9] N. Ernst, G. Bozdech, and J. H. Block, Surf. Sci. ECOSS I. Nederlands tijdeschrift voor vacuumtechniek **16**, 271 (1978).
[10] T. T. Tsong, Surf. Sci. **10**, 102 (1968).
[11] E. A. Moelwyn-Hughes, Physikal. Chemie, G. Thieme-Verlag, Stuttgart 1970, p. 367.
[12] J. P. Jones, Surf. Sci. **32**, 29 (1972).
[13] E. Sugata and T. Takeda, phys. Stat. Sol. **38**, 549 (1970).
[14] C. M. Lo and J. B. Hudson, Thin Solid Films **12**, 261 (1972). J. B. Hudson and C. M. Lo, Surf. Sci. **36**, 141 (1973).
[15] A. Y. Cho and C. D. Hendricks, J. Appl. Phys. **40**, 3339 (1969).
[16] E. Bauer, F. Bonczek, H. Poppa, and G. Todd, Surf. Sci. **53**, 87 (1975).
[17] W. Wüstner and G. Menzel, Thin Solid Films **24**, 211 (1974).
[18] W. Kollen and A. W. Czanderna, J. Colloid Interface Sci. **38**, 152 (1972).
[19] L. A. Petermann, Nuovo Cim. Supp. **5**, 364 (1967); Progress in Surf. Sci., Vol. 3, Part 1, Oxford 1972.
[20] R. Gomer, Solid State Phys. **30**, 132 (1975).
[21] L. Schmidt and R. Gomer, J. Chem. Phys. **42**, 3573 (1965).
[22] A. Hurkmans, E. G. Overbosch, and J. Los, Surf. Sci. **59**, 488 (1976).
[23] H. D. Beckey, Principles of Field Ionization and Field Desorption Mass Spectrometry, Pergamon Press, Oxford 1977.
[24] Gmelin Handbuch, Silber, 8. Aufl. Weinheim 1970, Bd. A2, 109.
[25] A. J. W. Moore and J. A. Spink, 21st Field Emission Symp. Marseille 1974.
[26] A. R. Waugh, E. D. Boyes, and M. J. Southon, Surf. Sci. **61**, 109 (1976).
[27] S. V. Krisnaswami and E. W. Müller, 22nd Field Emission Symp. Atlanta, Georgia 1975.
[28] D. G. Brandon, Phil. Mag. **14**, 803 (1966).
[29] W. A. Schmidt, O. Frank, and J. H. Block, Surf. Sci. **44**, 185 (1974).
[30] L. Ernst and J. H. Block, Surf. Sci. **49**, 333 (1975).
[31] F. Kirchner and H. Kirchner, Z. Naturforsch. **11a**, 718 (1965).